Anomalous Hall effect in antiferromagnetic Cr thin films

Hongyu Chen, Zexin Feng, Han Yan, Peixin Qin, Xiaorong Zhou, Huixin Guo, Xiaoning Wang, Haojiang Wu, Xin Zhang, Ziang Meng, and Zhiqi Liu*

School of Materials Science and Engineering, Beihang University, Beijing 100191, China

(Received 14 April 2021; revised 28 July 2021; accepted 28 July 2021; published 16 August 2021)

Bulk chromium is the simplest antiferromagnet in our general material database, which has been firmly believed to exhibit a collinear spin structure and a consequent vanishing anomalous Hall effect (AHE). In this work, we report an unexpected weak AHE in polycrystalline thin films of chromium. We attribute this phenomenon to the noncollinear spin textures induced by the local spin frustration and rearrangement in certain areas with high residual strain and defect densities. Moreover, a dominant underlying mechanism of intrinsic Berry phase is speculated. This could be a general feature for all the collinear antiferromagnetic thin-film materials with moderately high defect concentrations, making them promising candidates for emergent antiferromagnetic spintronics.

DOI: 10.1103/PhysRevB.104.064428

I. INTRODUCTION

The anomalous Hall effect (AHE), which has been universally observed in materials with a broken time-reversal symmetry (TRS) such as ferromagnets and ferrimagnets, can be ascribed to three main mechanisms [1]: the intrinsic contributions from topological Berry phase and the extrinsic contributions from skew scattering as well as side jump. Generally, in most antiferromagnets and paramagnets, the AHE vanishes due to their preserved (effective) TRS [2]. The survival of the AHE in such magnetic systems requires nontrivial spin configurations to break the TRS. For example, it has been demonstrated that k-space Berry phase can be induced by the nontrivial band structure of some antiferromagnets with noncollinear spin structures [3–7] or the spin chirality of certain frustrated magnets with noncoplanar spin orders [8,9], while real-space Berry phase can result from the spin chirality of large noncoplanar spin textures such as the skyrmion [10]. Both cases can give rise to a large intrinsic AHE (always termed as the topological Hall effect in the latter case). Also, the latest studies have revealed that the spin clusters in a frustrated magnet [11] or the localized magnetic moments in a paramagnetic heterostructure [12] can result in a huge AHE as well, which is dominated by the extrinsic skew-scattering mechanism.

On the other hand, recent studies have suggested that the spin structure of magnetic thin films might be somewhat different from that of bulks. For instance, first-principles analysis and spin-polarized scanning tunneling microscopy have revealed that the surface spins of the thin films of certain bulk collinear antiferromagnets such as Mn [13] and NiMn [14] could be reconstructed in a noncollinear manner due to surface induced frustration. Further, although it is unattainable to detect via conventional microscopies, the internal spin arrangement of thin films might be different from that of bulks as well owing to their residual strain and high defect densities [15]. However, hitherto, most scientific studies on magnetic thin-film materials have been conducted and interpreted based on the bulk spin structure, and the impact of such a possible spin-order divergence on physical properties has seldom drawn much attention.

Indeed, analogous to the nontrivial spins discussed above, such reconstructed spin configurations could be noncollinear and thus presumably break the local TRS and generate an exotic AHE as well, departing from the long-held perspective that the AHE is strictly prohibited in collinear antiferromagnets. Furthermore, during the past decades, it is owing to their lack of macroscopic magnetic moments and related beneficial properties that antiferromagnets have been regarded practically useless despite their well-known advantages such as faster spin dynamics and stronger stability under disturbance compared to ferromagnets [16,17]. Although recent breakthrough discoveries of the AHE in certain noncollinear antiferromagnets have substantially advanced emergent antiferromagnetic spintronics [3–7,18–21], such an intriguing AHE is permitted in only a few manganese alloys with triangular spin orders. In contrast, the long-termly neglected AHE mentioned above could be a universal feature for all the conductive antiferromagnetic thin-film materials regardless of their bulk spin structures, which would impart them with the potential for spintronic devices.

Motivated by the above understandings, we systematically investigated the Hall effect in polycrystalline thin films of chromium. Bulk Cr, the simplest elemental antiferromagnet in our general material database with a high Néel temperature (T_N) of ~311 K, has been firmly believed to exhibit a collinear spin structure [22] and a consequent vanishing AHE. Therefore, Cr could be the most readily fabricated material with an application perspective to demonstrate such an external-effect-induced AHE. As anticipated, a weak anomalous Hall resistivity signal of ~10 nΩ cm was observed in a 50-nm-thick sample. We proved that such an effect is an intrinsic attribute of polycrystalline Cr itself. Further, the AHE is found

*zhiqi@buaa.edu.cn

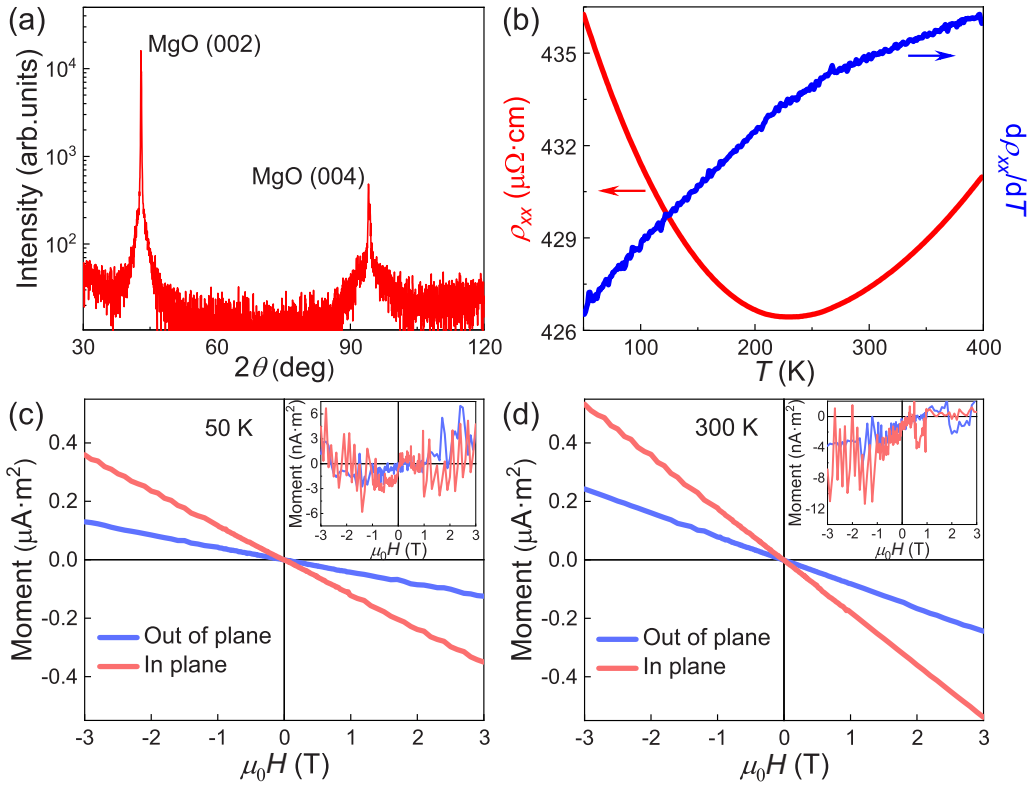

FIG. 1. (a) X-ray diffraction pattern, (b) temperature (T)-dependent longitudinal resistivity (ρ_{xx}) as well as $\mathrm{d}\rho_{xx}/\mathrm{d}T$, and moment versus in-plane and out-of-plane magnetic field at (c) 50 K and (d) 300 K of a Pt(2 nm)/Cr(50 nm)//MgO thin film. The insets show the moment data after subtracting linear backgrounds.

to be more pronounced in thinner films due to enhanced defect concentrations. Subtle as the AHE is, our observations could be both a reminder of the possibly changed spin structure for magnetic-thin-film studies and an implication of a feasible tactic to employ conductive collinear antiferromagnets as promising spintronic materials via microstructure modulation.

II. EXPERIMENTAL METHODS

All the films discussed in this article were fabricated by a d.c. magnetron sputtering system with a base pressure of $\sim 7.5 \times 10^{-9}$ Torr. During deposition, the sputtering power, Ar pressure and distance between targets and substrates were kept at 30 W, 3 mTorr, and 245 mm, respectively. The deposition rate of Cr was ~ 0.22 Å s^{-1}. The magnetic and transport properties of all the samples were measured via a Quantum Design VersaLab system. The standard four-probe method was employed to conduct both longitudinal and Hall resistance measurements [23]. During the Hall measurement, the applied current was modified from 0.5 to 5 mA in order to eliminate thermal effects while the magnetic field was programmed to sweep from $+3$ to -3 T then back to $+3$ T.

III. RESULTS AND DISCUSSION

Firstly, a 50-nm-thick Cr film was grown on a (001)-oriented MgO substrate at 300 °C. After the as-grown sample cooled down to room temperature, a 2-nm-thick platinum capping layer was deposited on it to preserve Cr from oxidization. The x-ray diffraction (XRD) pattern of this specimen is shown in Fig. 1(a). There is no observable diffraction peak except for those of MgO (002) and (004), suggesting the polycrystalline nature with a small grain size of the Cr layer. Temperature (T)-dependent longitudinal resistivity (ρ_{xx}) measured from 400 down to 50 K is depicted in Fig. 1(b). It is found that ρ_{xx} reaches its minimum of ~ 416 $\mu\Omega$ cm at $T_{\mathrm{m}} \approx 230$ K. Specifically, the film exhibits a semiconducting behavior with a negative temperature coefficient of resistivity (TCR) below T_{m} but a metallic-conducting characteristic with a positive TCR above T_{m}. Such a $\rho_{xx}(T)$ feature is analogous to that of an ion-beam-sputtered polycrystalline Cr film in a previous report [24], where the negative and positive TCR could be interpreted as a result of dominant scattering from disorder and phonons, respectively. In addition, although capped with a Pt layer, the polycrystalline Cr is highly resistive compared to its single-crystalline-bulk, epitaxial, and even other polycrystalline-film counterparts, which exhibit room-temperature ρ_{xx} values of ~ 13 $\mu\Omega$ cm [25], ~ 18 $\mu\Omega$ cm [26,27], and ~ 75 $\mu\Omega$ cm [24], respectively. The negative TCR at low temperatures together with the poor conductivity indicates a substantial disorder-scattering effect on the electrical transport properties, revealing the high defect concentrations of the sample.

In addition, it has been reported that a clear hump and concomitant minimum is usually observed in the $\rho_{xx}(T)$ and $\mathrm{d}\rho_{xx}/\mathrm{d}T$ curve of a high-quality Cr film, respectively, which corresponds to its paramagnetic-antiferromagnetic transition

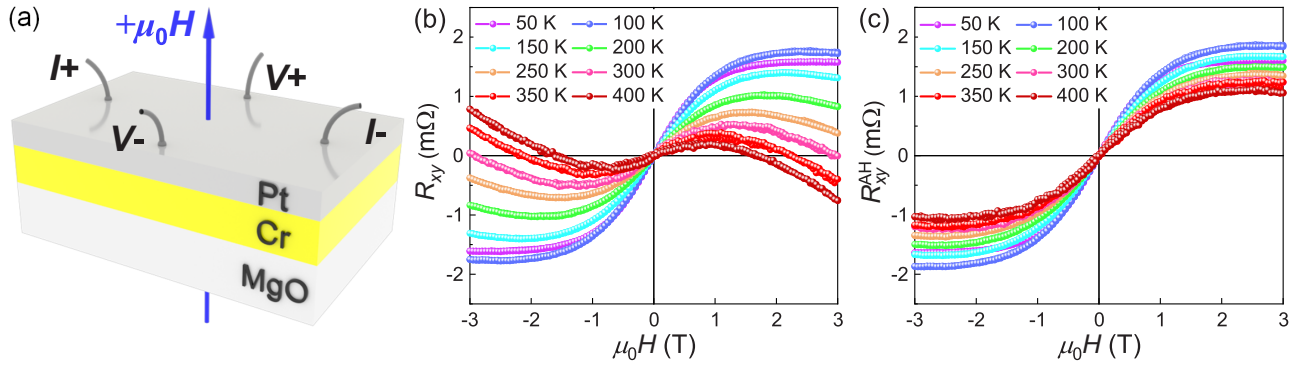

FIG. 2. (a) Schematic of the Hall measurement geometry. Magnetic-field-dependent (b) Hall resistance (R_{xy}) and (c) anomalous Hall resistance (R_{xy}^{AH}) deduced via subtracting the linear contribution from the ordinary Hall effect in (b) at $T = 50$–400 K of a Pt(2 nm)/Cr(50 nm)//MgO sample.

[26–29]. The T_N of a Cr thin film determined in this way varies with its substrate, thickness, deposition conditions, *etc*. depending on its residual strain, and could be dramatically different from the bulk value [28,29]. However, such an anomaly is concealed up to 400 K in our sample, which could be interpreted as a result of nonuniform internal-strain distribution [28]. We emphasize that the local T_N of certain regions in our film might be extremely high, since the intense crystal imperfection discussed above could induce a strong local stress, which would substantially imprint on its magnetic transition. In order to solidify its antiferromagnetism, the field-dependent magnetization of this sample was measured. As is illustrated in Figs. 1(c) and 1(d), only diamagnetic signals of MgO substrates were detected at 50 and 300 K. After subtracting the linear background, except for a subtle nonlinear contribution near zero field at 50 K, which is the common case for MgO [30], no other nonlinear signals of spurious moments were found within our measurement sensitivity, substantiating the antiferromagnetism of the Cr layer.

Subsequently, we investigated the Hall effect of this Pt(2 nm)/Cr(50 nm)//MgO specimen. Our measurement geometry is illustrated in Fig. 2(a). As is shown in Fig. 2(b), the Hall resistance (R_{xy}) exhibits a nonlinear dependence on the applied field (μ_0H) under $|\mu_0H| < 2.5$ T at $T = 50$–400 K. Generally, such an antisymmetric sideways S-shaped curve could be a mutual characteristic of two effects with completely different microscopic origins. Given that the Fermi surface of Cr is calculated to comprise both electron and hole pockets [22], apart from the AHE, it is reasonable to ascribe this feature to a multiple-band-induced ordinary Hall effect, where the nonlinearity results from a mixed Hall contribution from more than one conducting band under external magnetic fields. In addition, the sign reversion at 100 K of the Hall coefficient extracted from the high-field ($|\mu_0H| > 2.5$ T) data seems to be the sign of a multiband nature as well. However, the multiple-band effect generally manifests itself in multiband superconductors [31–33] or high-mobility systems such as two-dimensional electron gas [34,35] and semiconductors [36,37], which is inconsistent with our observation in Cr. Further, phenomenally, the exhibition of the nonlinear Hall response originated from such an effect usually requires a relatively low temperature ($T < 50$ K) [31–36] or a comparatively high magnetic field ($|\mu_0H| > 5$ T) [32,33,36,37]. In contrast, the nonlinear dependence of R_{xy} in our study is robust against a high T of 400 K but disappears above a low field of ±2.5 T, discordant with the multiple-band effect as well.

On the other hand, if we ascribe this phenomenon to the AHE, thus regarding the measured R_{xy} as a summation of both nonlinear anomalous Hall resistance (R_{xy}^{AH}) and linear ordinary Hall resistance (R_{xy}^{OH}), several advantageous features could be deduced. Figure 2(c) depicts the R_{xy}^{AH} component after subtracting the linear background in Fig. 2(b). Firstly, R_{xy}^{AH} seems to be approximate one order of magnitude larger than R_{xy}^{OH} at almost all the measurement temperatures. Moreover, the saturated magnetic field of R_{xy}^{AH} is practically independent of T. Additionally, the saturated R_{xy}^{AH} value exhibits a nonmonotonic variation with T and reaches its maximum at 100 K. These findings are reminiscent of the AHE in certain noncollinear antiferromagnets [4,20] but not so accordant with a multiple-band effect at any rate. Thus, hereafter we tentatively attribute our observation to the AHE while further evidence for the exclusion of the multiple-band effect will be displayed in the following paragraphs as we advance our study.

Given that the AHE in a collinear antiferromagnet is in contradiction to theoretical anticipations, one would naturally doubt whether it is an inherent attribute of Cr or simply stems from Pt, the interface between Cr and Pt, or other contamination. Indeed, it has been reported that ferromagnetism can be induced in an ultrathin Pt layer in contact with a ferromagnet or an antiferromagnet thanks to the magnetic proximity effect, which may give rise to the AHE [38–41]. Otherwise, the oxidization of Cr has been proposed to lead to the AHE as well [42], whose possibility has been already excluded in our study due to the existence of the AHE in a Pt-capped sample. In order to explore the exact origin of the observed AHE, we subsequently deposited a Cr(50 nm)//MgO and a Cu(2 nm)/Cr(50 nm)//MgO film under the same conditions as the Pt-capped one and examined their Hall responses. As is displayed in Figs. 3(a) and 3(b), a robust AHE signal survives in both specimens and exhibits similar features (such as the magnitude of R_{xy}^{AH}, T and μ_0H dependence of R_{xy}^{AH}, *etc*.) with the first sample. These observations indicate that the AHE in Cr films is practically independent of the capping

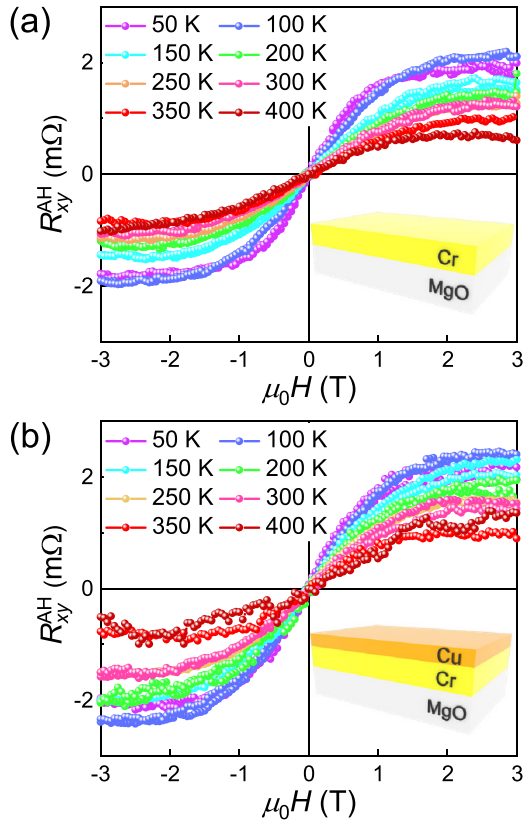

FIG. 3. R_{xy}^{AH} as a function of the applied field of (a) a Cr(50 nm)//MgO sample and (b) a Cu(2 nm)/Cr(50 nm)//MgO sample. The insets in (a) and (b) illustrate the corresponding film structure.

layer or the interface, thus revealing its major contribution from Cr.

Generally, the anomalous Hall resistivity (ρ_{xy}^{AH}) could be calculated as

$$\rho_{xy}^{AH} = \frac{V_{xy}^{AH}}{I_{xx}} t, \tag{1}$$

where I_{xx}, V_{xy}^{AH}, and t are the current flowing through Cr, the resultant anomalous Hall voltage and the thickness of Cr, respectively. In our study, although V_{xy}^{AH} could be readily deduced from the measured Hall voltage data, I_{xx} is hard to precisely determine, for the applied current would flow through both the Cr and the capping layer (if conductive). We proposed a method to estimate I_{xx} [43] and the obtained ρ_{xy}^{AH} data are shown in Fig. 4. The above three films exhibit comparable ρ_{xy}^{AH} values regardless of the capping layer, further confirming the negligible contribution to the AHE from oxidization or the magnetic proximity effect. Note that the maximum ρ_{xy}^{AH} value is ~12 nΩ cm, substantially smaller than that of bulk or thin-film samples of Mn_3Sn [4], Mn_3Ge [5,20], Mn_3Pt [6], and Fe [44]. The extremely small magnitude of the AHE suggests its unusual origin.

Additionally, armed with these conclusions, we could then check the applicability of the multiband origin of the "AHE" to our films by analyzing the ρ_{xx} values and the Hall resistivity (ρ_{xy}) − $\mu_0 H$ relation of the Cr(50 nm)//MgO sample based on a simple two-band model, for the contamination of its ρ_{xx} from oxidization is supposed to be negligible as well. In the two-band model, zero-field ρ_{xx} and $\rho_{xy}(\mu_0 H)$ under our measurement geometry are expressed as [37]

$$\rho_{xx} = \frac{1}{n_h \mu_h + n_e \mu_e}, \tag{2}$$

$$\rho_{xy} = -\frac{1}{e} \frac{\left(n_h \mu_h^2 - n_e \mu_e^2\right) + \mu_h^2 \mu_e^2 (\mu_0 H)^2 (n_h - n_e)}{(n_h \mu_h + n_e \mu_e)^2 + \mu_h^2 \mu_e^2 (\mu_0 H)^2 (n_h - n_e)^2} (\mu_0 H), \tag{3}$$

where n_e, n_h, μ_e, and μ_h are electron and hole densities and mobilities, respectively. When $\mu_0 H \to \infty$, Eq. (3) can be simplified as

$$\rho_{xy} = -\frac{1}{e} \frac{1}{(n_h - n_e)} (\mu_0 H), \tag{4}$$

which indicates a linear dependence of ρ_{xy} upon $\mu_0 H$ under a relatively high external field. Equipped with Eqs. (2) and (4), the order of magnitude of carrier densities as well as mobilities can be deduced in advance, which could serve as a constraint for fitting. Nevertheless, under such restricted conditions, we failed to fit the $\rho_{xy}(\mu_0 H)$ curves however we modified the parameters. Although the multiple-band effect cannot be completely ruled out at this stage, the non-self-consistency of the measured data in the two-band model suggests a prominent contribution to ρ_{xy} from the AHE at any rate.

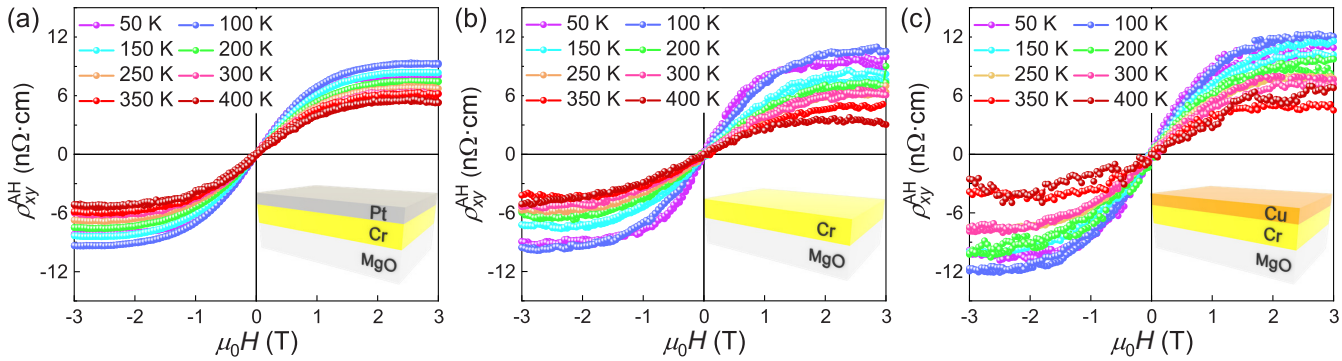

FIG. 4. Deduced ρ_{xy}^{AH} as a function of the applied field of (a) a Pt(2 nm)/Cr(50 nm)//MgO film, (b) a Cr(50 nm)//MgO film, and (c) a Cu(2 nm)/Cr(50 nm)//MgO film. The insets display the corresponding film structure.

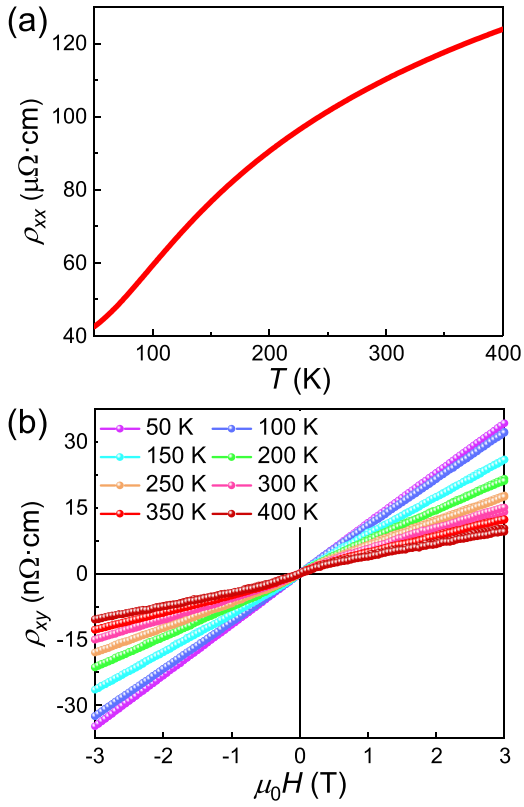

FIG. 5. (a) ρ_{xx}-T curve and (b) ρ_{xy} versus magnetic field at different temperatures of a postannealed Pt(2 nm)/Cr(50 nm)//MgO sample.

Note that the AHE is theoretically prohibited in an ideal antiferromagnetic Cr crystal while it is in the poorly crystallized thin films that a rather weak AHE appears. We were thus inspired to explore how this effect varies with crystallization. To this end, a 50-nm-thick Cr film was grown under the same conditions but annealed at 600 °C for 1 h before the deposition of a 2-nm-thick Pt-capping layer at room temperature. The transport properties of this sample are shown in Fig. 5. Although we still could not find any observable diffraction peak of Cr in the XRD measurement, the metallic conducting behavior as well as the dramatically reduced resistivity (∼112 $\mu\Omega$ cm at room temperature) indicates a substantially improved crystallization. Interestingly, as is displayed in Fig. 5(b), the AHE virtually vanishes in this film with almost linear ρ_{xy}-$\mu_0 H$ relations.

Generally, postannealing can release the residual strain and lower the defect densities of a thin film, which implies an underlying connection between the AHE and the microstructure of Cr. In addition, an epitaxial single-crystalline Pt-capped Cr(50 nm)//MgO sample was deposited at 500 °C for comparison, and no AHE signal was found at 50–400 K as expected. This further confirms that the AHE is related to the defects in antiferromagnetic Cr thin films and indicates that the rather weak nonlinearity in the $\rho_{xy}(\mu_0 H)$ curves of the postannealed sample could be due to the residual defects such as grain boundaries after annealing. Based on the previously mentioned studies that the magnetic properties and spin structures of thin films can be somewhat different from those of bulks [13–15], we speculate that the competition between the direct antiferromagnetic exchange interaction, residual strain, and other defects in a poorly crystallized Cr film could induce a local spin frustration in certain imperfectly arranged neighboring atoms. Such an effect might slightly tilt the nearby spins and generate a noncollinear spin configuration, whose subtle out-of-plane magnetization component can be stabilized only under finite magnetic fields, thus giving rise to a weak AHE with intrinsic and (or) extrinsic mechanisms, *i.e.*, the AHE in Cr films could be a summation of local contributions rather than an inherent attribute of the overall crystal. Hence it is no wonder that the observed AHE is rather subtle.

In order to examine the correlation between the AHE and defects, a series of Pt-capped thin films with thickness ranging from 20 to 100 nm were deposited. The average residual strain and defect concentrations of polycrystalline metallic thin films are supposed to reduce with increased film thickness [45–47]. This is corroborated in our study by the enhancement of the resistivity of the uncapped Cr films with decreased thickness due to rising defect scattering [Fig. 6(e)]. According to our proposal, since higher defect densities could induce larger spin-frustration regions, the AHE in Cr thin films is supposed to display a similar thickness dependence within moderate variation of defect concentrations.

As is illustrated in Figs. 6(a) and 6(b), compared with the 50-nm-thick specimen, the AHE is much more pronounced in the 20-nm-thick one with a maximum ρ_{xy}^{AH} value of ∼82 nΩ cm but practically undetectable in the 100-nm-thick one as anticipated. Note that for the latter sample, the Hall coefficient reverses its sign with increased T, suggesting that the dominant carriers alter from electrons at $T \leqslant 150$ K to holes at $T \geqslant 200$ K under our measurement geometry. In view of the complex Fermi surface of Cr [22], this could be due to the change of band filling with T and the resultant variation of carrier densities and mobilities. Although such a phenomenon is the feature of multiband systems, nonlinearity is absent in all the $\rho_{xy}(\mu_0 H)$ curves of this sample, indicating an ignorable contribution to the AHE from the multiple-band effect once more.

Further, ρ_{xy}^{AH} monotonically decreases with increased thickness at all the measurement temperatures as displayed in Fig. 6(c), which is consistent with our expectations as well. Indeed, ρ_{xy}^{AH} is always positively related to ρ_{xx} [1], and is thus not appropriate enough to reflect the divergence of the AHE with different defect concentrations. On the other hand, the Hall angle (θ_{H}), which is defined as $\tan\theta_{\mathrm{H}} = \sigma_{xy}/\sigma_{xx}$, can be interpreted as the longitudinal-transverse current-conversion efficiency in the AHE. Therefore, we additionally employed $\tan\theta_{\mathrm{H}}$ to qualitatively compare the AHE of different Cr films. As is shown in Fig. 6(d), $\tan\theta_{\mathrm{H}}$ exhibits an analogous thickness dependence to that of ρ_{xy}^{AH}, in good accordance with our anticipation, which indicates that the AHE is indeed related to the strain and defects in thin films. Additionally, the intense variation of the AHE with film thickness provides extra evidence that the contribution to ρ_{xy} from the multiple-band effect is negligible since it is supposed to be inherent and independent of the volume of Cr.

Nevertheless, the specific dominant mechanism of this AHE remains elusive. It has been demonstrated that nontrivial

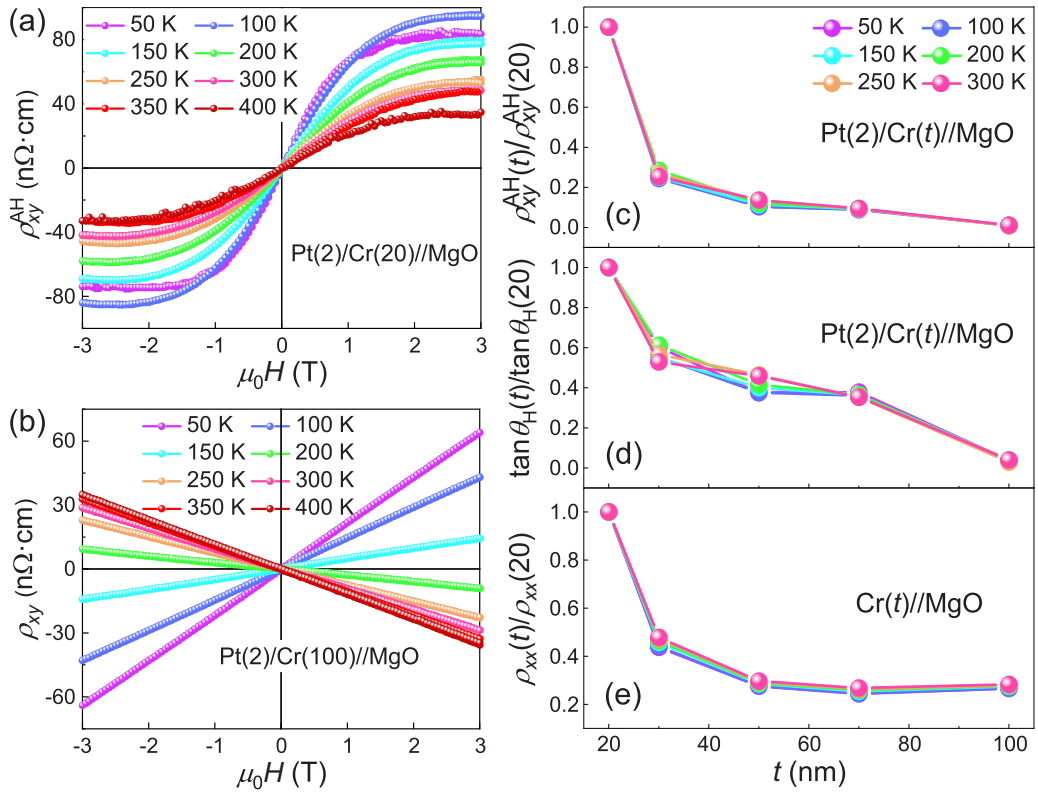

FIG. 6. (a) Magnetic-field dependent ρ_{xy}^{AH} of a Pt(2 nm)/Cr(20 nm)//MgO sample. (b) ρ_{xy} versus magnetic field of a Pt(2 nm)/Cr (100 nm)//MgO film. Thickness (t)-dependent relative values of (c) ρ_{xy}^{AH} and (d) tangent Hall angle ($\tan\theta_H$) of Pt(2 nm)/Cr(t)//MgO and (e) ρ_{xx} of Cr(t)//MgO films with respect to those of a platinum-capped and an uncapped 20-nm-thick film, respectively.

spin structures could result in both an intrinsic AHE with k-space [4–6] or real-space [8,9] Berry-phase mechanisms and an extrinsic AHE with skew-scattering origins [11,12]. Phenomenally, the AHE of Cr films resembles that in noncollinear antiferromagnets such as Mn_3Sn [4] and Mn_3Ge [20] particularly in the nonmonotonic dependence of saturated ρ_{xy}^{AH} on T and the T-independent saturated field of ρ_{xy}^{AH}, which indicates an intrinsic origin from k-space Berry phase. Also, recent reports have suggested a connection between the ρ_{xy}^{AH}-T relation and the evolution of the magnetic structure of Mn_3Sn [48,49], which seems applicable to our samples as well, for it is natural to assume that the frustrated spin structure could vary with T and the debility of the AHE at high temperatures could be interpreted as their partial vanishment due to enhanced thermal fluctuations. On the other hand, if we ascribe all the AHE signal to the k-space-Berry-phase mechanism, according to the well-established scaling analysis of the AHE in ferromagnets [50], $\rho_{xy}^{AH} \propto \rho_{xx}^{0.4}$ is expected for our highly resistive Cr films [here ρ_{xy}^{AH} is defined as the saturated value of $\rho_{xy}^{AH}(\mu_0 H)$ at 3 T and a certain T]. However, we failed to extract such a power-law relation from our results. The departure from the scaling relation could result from the existence of the spin-texture-induced topological Hall effect [51]. In addition, the extrinsic contributions from the skew-scattering mechanism are presumed to be negligible in our study, for it is proposed to dominate only in clean systems with relatively high conductivity [50].

IV. CONCLUSIONS

In summary, a weak AHE with a ρ_{xy}^{AH} value of ∼10 nΩ cm was observed in a 50-nm-thick polycrystalline Cr thin film. This effect is demonstrated to be an intrinsic attribute of Cr owing to its independence on the capping layer. In addition, the AHE practically vanishes in a postannealed sample but is much more pronounced in thinner films with ρ_{xy}^{AH} increasing to ∼82 nΩ cm at a thickness of 20 nm, indicating its intimate correlation with the defects in thin films. We propose that local spin frustration could be induced by poor crystallinity, breaking the local TRS and thus giving rise to such a subtle AHE. However, the dominant mechanism of this effect remains elusive. According to its phenomenal analogy to that in certain noncollinear antiferromagnets, an intrinsic Berry-phase origin is speculated. These observations shed light on the impact of possible spin-structure changes in thin films and could be a general feature for all the collinear antiferromagnetic thin-film materials, which might pave the way for their future application in antiferromagnetic spintronics. For example, the exotic noncollinear spin structure of Cr films could be further controlled by low-power electric fields [52–58].

ACKNOWLEDGMENTS

Z.L. acknowledges financial support by the National Natural Science Foundation of China (Grants No. 51822101, No. 51861135104, and No. 51771009).

[1] N. Nagaosa, J. Sinova, S. Onoda, A. H. MacDonald, and N. P. Ong, Rev. Mod. Phys. **82**, 1539 (2010).

[2] L. Šmejkal, R. González-Hernández, T. Jungwirth, and J. Sinova, Sci. Adv. **6**, eaaz8809 (2020).

[3] H. Chen, Q. Niu, and A. H. MacDonald, Phys. Rev. Lett. **112**, 017205 (2014).

[4] S. Nakatsuji, N. Kiyohara, and T. Higo, Nature (London) **527**, 212 (2015).

[5] A. K. Nayak, J. E. Fischer, Y. Sun, B. Yan, J. Karel, A. C. Komarek, C. Shekhar, N. Kumar, W. Schnelle, J. Kübler *et al.*, Sci. Adv. **2**, e1501870 (2016).

[6] Z. Q. Liu, H. Chen, J. M. Wang, J. H. Liu, K. Wang, Z. X. Feng, H. Yan, X. R. Wang, C. B. Jiang, J. M. D. Coey *et al.*, Nat. Electron. **1**, 172 (2018).

[7] J. Kübler and C. Felser, EPL **108**, 67001 (2014).

[8] Y. Taguchi, Y. Oohara, H. Yoshizawa, N. Nagaosa, and Y. Tokura, Science **291**, 2573 (2001).

[9] Y. Machida, S. Nakatsuji, S. Onoda, T. Tayama, and T. Sakakibara, Nature (London) **463**, 210 (2010).

[10] A. Neubauer, C. Pfleiderer, B. Binz, A. Rosch, R. Ritz, P. G. Niklowitz, and P. Böni, Phys. Rev. Lett. **102**, 186602 (2009).

[11] S.-Y. Yang, Y. Wang, B. R. Ortiz, D. Liu, J. Gayles, E. Derunova, R. Gonzalez-Hernandez, L. Šmejkal, Y. Chen, S. S. P. Parkin *et al.*, Sci. Adv. **6**, eabb6003 (2020).

[12] D. Maryenko, A. S. Mishchenko, M. S. Bahramy, A. Ernst, J. Falson, Y. Kozuka, A. Tsukazaki, N. Nagaosa, and M. Kawasaki, Nat. Commun. **8**, 14777 (2017).

[13] C. L. Gao, U. Schlickum, W. Wulfhekel, and J. Kirschner, Phys. Rev. Lett. **98**, 107203 (2007).

[14] C. L. Gao, A. Ernst, A. Winkelmann, J. Henk, W. Wulfhekel, P. Bruno, and J. Kirschner, Phys. Rev. Lett. **100**, 237203 (2008).

[15] D. Sander, J. Phys.: Condens. Matter **16**, R603 (2004).

[16] T. Jungwirth, X. Marti, P. Wadley, and J. Wunderlich, Nat. Nanotechnol. **11**, 231 (2016).

[17] V. Baltz, A. Manchon, M. Tsoi, T. Moriyama, T. Ono, and Y. Tserkovnyak, Rev. Mod. Phys. **90**, 015005 (2018).

[18] X. Wang, Z. Feng, P. Qin, H. Yan, X. Zhou, H. Guo, Z. Leng, W. Chen, Q. Jia, Z. Hu *et al.*, Acta Mater. **181**, 537 (2019).

[19] H. Guo, Z. Feng, H. Yan, J. Liu, J. Zhang, X. Zhou, P. Qin, J. Cai, Z. Zeng, X. Zhang *et al.*, Adv. Mater. **32**, 2002300 (2020).

[20] P. Qin, Z. Feng, X. Zhou, H. Guo, J. Wang, H. Yan, X. Wang, H. Chen, X. Zhang, H. Wu *et al.*, ACS Nano **14**, 6242 (2020).

[21] H. Tsai, T. Higo, K. Kondou, T. Nomoto, A. Sakai, A. Kobayashi, T. Nakano, K. Yakushiji, R. Arita, S. Miwa *et al.*, Nature (London) **580**, 608 (2020).

[22] E. Fawcett, Rev. Mod. Phys. **60**, 209 (1988).

[23] See Supplemental Material at http://link.aps.org/supplemental/10.1103/PhysRevB.104.064428 for the details of the resistivity determination of a plain film and the comparation with the Hall-bar method.

[24] M. Ohashi, K. Ohashi, M. Sawabu, M. Miyagawa, T. Kubota, and K. Takanashi, Phys. Lett. A **380**, 3133 (2016).

[25] S. Arajs, R. V. Colvin, and M. J. Marcinkowski, J. Less-Common Met. **4**, 46 (1962).

[26] R. K. Kummamuru and Y.-A. Soh, Nature (London) **452**, 859 (2008).

[27] M. Ohashi, M. Sawabu, H. Nakanishi, K. Ohashi, and K. Maeta, Phys. B **536**, 790 (2018).

[28] A. A. Milgram and C. s. Lu, J. Appl. Phys. **39**, 2851 (1968).

[29] J. A. J. Lourens, S. Arajs, H. F. Helbig, L. Cheriet, and E. S. A. Mehanna, J. Appl. Phys. **63**, 4282 (1988).

[30] L. Balcells, J. I. Beltrán, C. Martínez-Boubeta, Z. Konstantinović, J. Arbiol, and B. Martínez, Appl. Phys. Lett. **97**, 252503 (2010).

[31] H. Yang, Y. Liu, C. Zhuang, J. Shi, Y. Yao, S. Massidda, M. Monni, Y. Jia, X. Xi, Q. Li *et al.*, Phys. Rev. Lett. **101**, 067001 (2008).

[32] H. Lei, D. Graf, R. Hu, H. Ryu, E. S. Choi, S. W. Tozer, and C. Petrovic, Phys. Rev. B **85**, 094515 (2012).

[33] Y. Sun, T. Taen, T. Yamada, S. Pyon, T. Nishizaki, Z. Shi, and T. Tamegai, Phys. Rev. B **89**, 144512 (2014).

[34] J. S. Kim, S. S. A. Seo, M. F. Chisholm, R. K. Kremer, H.-U. Habermeier, B. Keimer, and H. N. Lee, Phys. Rev. B **82**, 201407(R) (2010).

[35] X. Renshaw Wang, L. Sun, Z. Huang, W. M. Lü, M. Motapothula, A. Annadi, Z. Q. Liu, S. W. Zeng, T. Venkatesan, and Ariando, Sci. Rep. **5**, 18282 (2015).

[36] Y. Luo, H. Li, Y. M. Dai, H. Miao, Y. G. Shi, H. Ding, A. J. Taylor, D. A. Yarotski, R. P. Prasankumar, and J. D. Thompson, Appl. Phys. Lett. **107**, 182411 (2015).

[37] C. Wang, L. Chen, Z. Liu, Z. Liu, X.-L. Ma, C. Xu, H.-M. Cheng, W. Ren, and N. Kang, Adv. Electron. Mater. **5**, 1800839 (2019).

[38] S. Y. Huang, X. Fan, D. Qu, Y. P. Chen, W. G. Wang, J. Wu, T. Y. Chen, J. Q. Xiao, and C. L. Chien, Phys. Rev. Lett. **109**, 107204 (2012).

[39] Y. M. Lu, Y. Choi, C. M. Ortega, X. M. Cheng, J. W. Cai, S. Y. Huang, L. Sun, and C. L. Chien, Phys. Rev. Lett. **110**, 147207 (2013).

[40] Y. Cheng, S. Yu, M. Zhu, J. Hwang, and F. Yang, Phys. Rev. Lett. **123**, 237206 (2019).

[41] M. Asa, C. Autieri, R. Pazzocco, C. Rinaldi, W. Brzezicki, A. Stroppa, M. Cuoco, G. Varvaro, S. Picozzi, and M. Cantoni, Phys. Rev. Research **2**, 043394 (2020).

[42] D. Qu, S. Y. Huang, and C. L. Chien, Phys. Rev. B **92**, 020418(R) (2015).

[43] In order to figure out I_{xx} for each capped sample, we employed an uncapped Cr film with the same thickness as a reference to judge whether the capping layer is conductive. Since transport properties of the uncapped film and the Cr layer in the capped one are supposed to be close to each other, a substantially higher resistance of the former could suggest a well-conductive capping layer in the latter. For a sample with a well-conductive capping layer, suppose the resistance of Cr is the same as that of the uncapped film, then I_{xx} and consequent ρ_{xy}^{AH} could be roughly evaluated based on a simple parallel-electrical-connection model.

[44] Y. Tian, L. Ye, and X. Jin, Phys. Rev. Lett. **103**, 087206 (2009).

[45] J. W. C. De Vries, Thin Solid Films **167**, 25 (1988).

[46] G. C. A. M. Janssen, Thin Solid Films **515**, 6654 (2007).

[47] R. Daniel, K. J. Martinschitz, J. Keckes, and C. Mitterer, Acta Mater. **58**, 2621 (2010).

[48] Y. Song, Y. Hao, S. Wang, J. Zhang, Q. Huang, X. Xing, and J. Chen, Phys. Rev. B **101**, 144422 (2020).

[49] J. M. Taylor, A. Markou, E. Lesne, P. K. Sivakumar, C. Luo, F. Radu, P. Werner, C. Felser, and S. S. P. Parkin, Phys. Rev. B **101**, 094404 (2020).

[50] S. Onoda, N. Sugimoto, and N. Nagaosa, Phys. Rev. B **77**, 165103 (2008).

[51] N. Kanazawa, Y. Onose, T. Arima, D. Okuyama, K. Ohoyama, S. Wakimoto, K. Kakurai, S. Ishiwata, and Y. Tokura, Phys. Rev. Lett. **106**, 156603 (2011).

[52] Z. Q. Liu, L. Li, Z. Gai, J. D. Clarkson, S. L. Hsu, A. T. Wong, L. S. Fan, M. W. Lin, C. M. Rouleau, T. Z. Ward *et al.*, Phys. Rev. Lett. **116**, 097203 (2016).

[53] Z. Q. Liu, J. H. Liu, M. D. Biegalski, J. M. Hu, S. L. Shang, Y. Ji, J. M. Wang, S. L. Hsu, A. T. Wong, M. J. Cordill *et al.*, Nat. Commun. **9**, 41 (2018).

[54] Z. Feng, H. Yan, and Z. Liu, Adv. Electron. Mater. **5**, 1800466 (2019).

[55] Z. Liu, Z. Feng, H. Yan, X. Wang, X. Zhou, P. Qin, H. Guo, R. Yu, and C. Jiang, Adv. Electron. Mater. **5**, 1900176 (2019).

[56] H. Yan, Z. Feng, S. Shang, X. Wang, Z. Hu, J. Wang, Z. Zhu, H. Wang, Z. Chen, H. Hua *et al.*, Nat. Nanotechnol. **14**, 131 (2019).

[57] Z. Feng, H. Yan, X. Wang, H. Guo, P. Qin, X. Zhou, Z. Chen, H. Wang, Z. Jiao, Z. Leng *et al.*, Adv. Electron. Mater. **6**, 1901084 (2020).

[58] H. Yan, Z. Feng, P. Qin, X. Zhou, H. Guo, X. Wang, H. Chen, X. Zhang, H. Wu, C. Jiang *et al.*, Adv. Mater. **32**, 1905603 (2020).